New Mathematical Approaches for Image Reconstruction in the Oil and Medical Industries

M. Moscoso

Gregorio Millán Institute, Universidad Carlos III de Madrid, Leganés 28911, Spain, moscoso@math.uc3m.es

Summary. The problem of reconstructing images from measurements at the boundary of a domain belongs to the class of inverse problems. Although in different applications the techniques used to create the images work under different physical principles and map different physical parameters, they all share similar mathematical foundations. I will present here two mathematical approaches for image reconstruction. The first one is used to solve the so called history matching problem in the oil industry, and the second one is specially designed for the application of optical molecular imaging in biomedicine.

1 Introduction

Imaging is a broad field which covers all aspects of the analysis, modification, compression, visualization, and generation of images. There are at least two major areas in imaging science in which applied mathematics has a strong impact: image processing, and image reconstruction. In image processing the input is a (digital) image such as a photograph, while in image reconstruction the input is the data gathered on the boundary of an object. In the latter case, the data is limited, and its poor information content is not enough to generate an image to start with.

Image processing techniques apply numerical algorithms to either improve a given image or to extract information about the image [1]. Image segmentation is typically used for the latter purpose. It refers to the process of partitioning an image into multiple regions (locating objects and boundaries) in order to simplify its representation for its further analysis. Each region shares the same properties or characteristics such as color, intensity or texture. Different techniques have been applied for image segmentation. We mention here, graph partitioning methods in which the image is modelled as a graph; level-set methods in which an initial shape is evolved towards the object boundary; and statistical methods in which we view a region of an image as one realization of a random process (probability distribution functions and

A.D. Fitt et al. (eds.), *Progress in Industrial Mathematics at ECMI 2008*, Mathematics in Industry 15, DOI 10.1007/978-3-642-12110-4_2,

histograms are used to estimate the characteristics of the regions). We will not discuss the mathematics of image processing here.

On the other hand, image reconstruction refers to the techniques used to create an image of the interior of a body from data collected on its boundary [2]. Mathematically, an image reconstruction can be seen as the solution of an inverse problem in which the cause is inferred from the effect. We will show here two different applications in the oil and medical industries. The first application is the so called history matching problem where we want to estimate the unknown properties of a reservoir, such as its porosity and permeability, from the production data. We will apply to this problem an adjoint technique. The second application is the inverse fluorescent source problem in optical molecular imaging. We obtain here explicit solutions for a point source and a voxel source from which we estimate the location, size and total strength of a general source.

The goal of this paper is to illustrate the role of the imaging techniques in these applications. In the oil industry, for example, they improve our ability to design a good management strategy to increase the productivity and life of a reservoir. They help to better understand the reservoir behavior so that its performance can be predicted and controlled with higher reliability. On the other hand, in the biomedical application of optical molecular imaging they are used to monitor cellular and structural changes associated with predisease states such as dysplastic progression.

2 Reservoir Characterization

Oil fields typically extend over large areas, possibly several hundred kilometers across and full exploitation entails multiple wells scattered across the area. Initially, the natural differential pressure displaces hydrocarbons from the reservoir, into the wellbore and up to the surface. This is the primary recovery stage. As oil production takes place, the reservoir pressure declines, and eventually, the primary recovery stage reaches its limit. Typically, only a small fraction, around the 15% of the initial oil in place is produced during the primary recovery stage. During the second stage, water is injected into the production zone to sweep the oil from the reservoir. The secondary recovery stage reaches its limit when the injected fluid is produced in considerable amounts at the production wells and the production is no longer economical. Around 40% of the field's oil is produced during this stage. The third stage of oil production uses sophisticated techniques that alter the original properties of the oil. Its purpose is to improve oil displacement or fluid flow in the reservoir. It allows another 10% of the filed's oil to be recovered.

We consider here the case of 'secondary recovery' where water is injected through several injection wells conveniently located in order to enhance oil production. Potential problems associated with waterflood techniques include

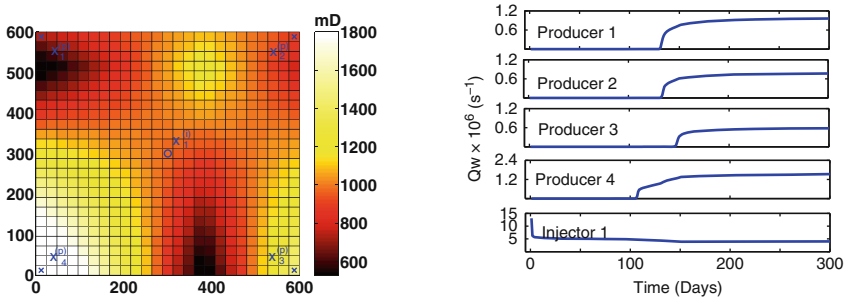

Fig. 1. (**a**) Permeability distribution: 5-spot example; (**b**) extracted water flows at the producers (shown in figure (**a**) with x's) and injected water flow at the injector (shown in figure (**a**) with a *circle*)

inefficient recovery due to the unknown variable permeability, that is due to the impact of the unknown geological heterogeneity on flow during oil recovery. Therefore, there is a need to estimate the permeability distribution inside the reservoir in order to optimize oil production. Proper characterization of the reservoir heterogeneity helps to better understand the reservoir behavior so its performance can be predicted and controlled with higher reliability.

2.1 The Direct Problem: Governing Equations

Secondary oil recovery techniques involve the simultaneous flow of up to three fluid phases. It requires the solution of the equations of a multiphase flow in a porous medium. We will consider here only water and oil, and we will neglect gas. We will also neglect the effects of gravity and capillary pressure. For describing the flow dynamics in the reservoir $\Omega \subset \mathbb{R}^n$ (n $= 2, 3$), we use a simplified Black-Oil model [3]:

$$-\nabla \cdot \Big[T \nabla p\Big] = Q, \qquad \text{in} \quad \Omega \times [0, t_f], \tag{1}$$

$$\phi \frac{\partial S_w}{\partial t} - \nabla \cdot \big[T_w \nabla p\big] = Q_w, \qquad \text{in} \quad \Omega \times [0, t_f], \tag{2}$$

where $p(\mathbf{x}, t)$ and $S_w(\mathbf{x}, t)$ are the unknowns of the problem which represent the pressure and the water saturation at position $\mathbf{x}$ and time t, respectively. The water saturation S_w measures the volume fraction of water. $\phi(\mathbf{x})$ is the porosity, and T and T_w are the transmissibilities, which are known functions which depend linearly on the permeability K, the parameter to be reconstructed, and nonlinearly on S_w,

$$T_w = K(\mathbf{x}) \frac{K_{rw}(S_w)}{\mu_w}, \quad T_o = K(\mathbf{x}) \frac{K_{ro}(S_w)}{\mu_o}, \quad T = T_w + T_o. \tag{3}$$

$K_{rw}(S_w)$, $K_{ro}(S_w)$, μ_w and μ_o denote the relative permeabilities and the viscosities of each phase, respectively. Hereafter, the subscript 'w' stands for 'water', while the subscript 'o' stands for 'oil'. $Q(\mathbf{x},t)$ and $Q_w(\mathbf{x},t)$ define the total flow and the water flow at the wells, respectively. They are given by

$$Q = cT\sum_{j=1}^{N_i}(p_{wb_j}^{(i)} - p)\delta(\mathbf{x}-\mathbf{x}_j^{(i)}) + cT\sum_{j=1}^{N_p}(p_{wb_j}^{(p)} - p)\delta(\mathbf{x}-\mathbf{x}_j^{(p)}), \tag{4}$$

$$Q_w = cT\sum_{j=1}^{N_i}(p_{wb_j}^{(i)} - p)\delta(\mathbf{x}-\mathbf{x}_j^{(i)}) + cT_w\sum_{j=1}^{N_p}(p_{wb_j}^{(p)} - p)\delta(\mathbf{x}-\mathbf{x}_j^{(p)}), \tag{5}$$

where $\mathbf{x}_j^{(i)}$, $j=1,\ldots,N_i$, denote the locations of the N_i injector wells, $\mathbf{x}_j^{(p)}$, $j=1,\ldots,N_p$, denote the locations of the N_p production wells, and $p_{wb_j}^{(i)}$, $p_{wb_j}^{(p)}$ are the imposed well bore pressures at the N_i injector wells and at the N_p production wells, respectively. Here, c is a constant that depends on the well model. Since $p_{wb_j}^{(i)}$ ($p_{wb_j}^{(p)}$) are larger (smaller) than the reservoir pressure at the injector (production) wells, Q and Q_w are positive (negative) at the injector (production) wells.

Equation (2) is the conservation law for water in a porous medium and (1) is obtained by combining the conservation laws for water and oil in order to eliminate the time derivative term. It is assumed that the flow obeys Darcy's law ($\mathbf{u}_l(\mathbf{x},t) = -\frac{K(\mathbf{x})K_{rl}(S_w)}{\mu_l}\nabla p(\mathbf{x},t), l=w,o$) which defines the velocity of each phase in the medium. Equations (1) and (2) are solved with the following initial and boundary conditions:

$$S_w(\mathbf{x},0) = S_w^0(\mathbf{x}) \qquad \text{in} \quad \Omega, \tag{6}$$

$$p(\mathbf{x},0) = p^0(\mathbf{x}) \qquad \text{in} \quad \Omega, \tag{7}$$

$$\nabla p\cdot\boldsymbol{\nu} = 0 \qquad \text{on} \quad \partial\Omega, \tag{8}$$

where $\boldsymbol{\nu}$ is the outward unit normal to $\partial\Omega$. The boundary condition (8) implies no flux across the boundary.

Equations (1)–(8) define the *direct problem* for the dynamic production history at the extraction wells. It refers to the resolution of the equations describing the flow within the reservoir assuming that the properties of the porous media, defined by $K(\mathbf{x})$ and $\phi(\mathbf{x})$, are known. The properties of the fluids are defined by μ_w, μ_o, $K_{rw}(S_w)$, and $K_{ro}(S_w)$. The well bore pressures $p_{wb_j}^{(i,p)}$ are known functions of time at the well's positions.

The left side of Fig. 1 shows a five-spot layout with an injector well (o) in the center (location $\mathbf{x}_1^{(i)}$) and four production wells (x) at the corners of a two-dimensional reservoir (locations $\mathbf{x}_j^{(p)}$, $j=1\ldots4$, being $j=1$ the well in the upper left corner and numbered in the clockwise direction). Also shown is the real permeability distribution in milli-Darcys (mD). The water injected at the injection well displaces the oil in the reservoir towards the production

wells. Time resolution of the flow equations provides the time evolution of pressure and flow at each point of the reservoir. Of particular interest is the oil and water flow rate at each production well. The right hand side of Fig. 1 shows the time history of water flow rate (Q_w) at each well obtained by solving the direct problem. Notice that water arrival occurs first at well four since it is surrounded by a region of high permeability.

2.2 The Inverse Problem: The Adjoint Method

In the *inverse problem* we assume that the water flow rate at each well is known but the permeability distribution is unknown. Hence, the unknown of interest in the inverse problem is the permeability K that we want to estimate from the water production rates. We will start with an initial permeability guess (typically some constant distribution) and will iteratively modify it until the actual water production rate at each well is matched by the simulator.

Adjoint techniques are particularly useful in large scale inverse problems where relatively few independent experiments can be performed for gathering data but many parameters need to be reconstructed. Since typically only one experiment is performed in history matching due to the simultaneous production process, the adjoint technique is therefore much faster in this application. Adjoint techniques have also been applied with great success in other applications of geophysical and medical imaging (see [2], and references therein). Other techniques have also been applied to the history matching problem. Among them, we mention shape-based reconstructions that use level-set techniques [4,5].

The forward operator described in the previous section can be written in abstract form as

$$M : P \longrightarrow D, \qquad M[K] = Q_w[K]|_{\Omega_+ \times [0,t_f]}, \tag{9}$$

where Q_w is obtained by solving the direct problem for a given permeability distribution K (1)–(8). Here, we denote the space of permeability distributions K by P, the data space by D, and the set of measurement locations ('well-locations') by $\Omega_+ := \{\mathbf{x}_1^{(p)}, \mathbf{x}_2^{(p)}, \ldots, \mathbf{x}_{N_p}^{(p)}\}$. At each of these positions, the water flow is measured during a time $0 \leq t \leq t_f$, such that the data space D is given by $D = (L_2([0, t_f]))^{N_p}$.

For some guess K of the permeability, and given the measured data $\tilde{G}$ (water flow rate) at these production wells, we also define the residual operator

$$R[K] = M[K] - \tilde{G}. \tag{10}$$

Equation (10) describes the mismatch between the physically measured data and the data corresponding to a guess K. In the inverse problem, we ideally want to find a permeability distribution $\hat{K}$ in P such that

$$R[\hat{K}] = 0. \tag{11}$$

This equation has a solution in the situation where the data $\tilde{G}$ are in the range of M. Most likely this is not the case if we use real data, so we generalize our criterion for a solution defining the least squares cost functional

$$\mathcal{J}(K) = \frac{1}{2}\|R(K)\|^2, \tag{12}$$

and searching for a minimizer of this cost functional. This cost functional defines the differences between the predicted model (as described by K) and the actual observed measurements in an L_2 norm sense.

In order to find an 'update' δK for our permeability K we linearize (in a Newton-type fashion) the nonlinear operator R (assuming that this linearized operator $R'[K]$ exists and is well-defined) and write

$$R[K + \delta K] = R[K] + R'[K]\delta K + 0(||\delta K||^2), \tag{13}$$

where the linearized operator $R'[K]$ represents the Frechet derivative of R at K, which is closely related to the 'sensitivity functions' of the parameter profile with respect to the data. Using (13) we want to look for a correction δK such that $R[K + \delta K] = 0$. Neglecting terms of order $0(||\delta K||^2)$ in (13), this amounts to solving

$$R'[K]\delta K = -R[K]. \tag{14}$$

A classical solution to the ill-posed linear inverse problem (14) is the minimum-norm solution

$$\delta K_{MN} = -R'[K]^* \left(R'[K]R'[K]^*\right)^{-1} R[K], \tag{15}$$

where $R'[K]^*$ represents the adjoint operator of $R'[K]$. In our application, the operator $C = (R'[K]R'[K]^*)^{-1}$ is ill-conditioned and expensive to calculate, so it will be replaced by the identity operator I (note that C 'just' maps vectors from the data space back into the data space, so it can be considered as a 'filtering operator'). Therefore, we end up with simply applying the adjoint operator $R'[K]^*$ to the residuals R for calculating the update direction

$$\delta K = -R'[K]^* R[K]. \tag{16}$$

Note that the operator $R'[K]^*$ maps the residuals back into the parameter space for obtaining the update. Therefore, in order to determine δK in each step from (16), we will need an efficient method for applying $R'[K]^*$ to a given vector ρ of the data space. Next, we show how to compute it (the details can be found in [6]).

Let us consider a small perturbation δK in the permeability distribution K that leads to small perturbations W and q in the saturation and the pressure, respectively. Here we assume that the pressure remains nearly unchanged so that ∇q is negligible. This is so because the pressure is a smooth function compared to the saturation. Using a heuristic approach to derive an expression

for R', we introduce $K + \delta K$ and $S_w + W$ in (2) and we neglect second order terms. Then, W solves the initial value problem

$$\phi \frac{\partial W}{\partial t} - \nabla \cdot \big[\frac{\partial T_w}{\partial S_w} W \nabla p\big] - \frac{\partial Q_w}{\partial S_w} W = \frac{\delta K}{K} Q_w + \nabla \cdot \big[\frac{\delta K}{K} T_w \nabla p\big] \quad \text{in } \Omega \tag{17}$$

$$W(\mathbf{x}, 0) = 0 \qquad \text{in } \Omega \tag{18}$$

where S_w and p are the solutions of (1)–(8). From the value of W we derive the linearized response of the data to a perturbation δK in the permeability distribution, which is given by

$$R'[K]\delta K = \frac{\partial Q_w}{\partial S_w} W \Big|_{\Omega_+ \times [0, t_f]} . \tag{19}$$

The adjoint operator $R'[K]^*$ is defined by

$$\langle R'[K]\delta K, \rho \rangle_D = \langle \delta K, R'[K]^* \rho \rangle_P , \tag{20}$$

where $\langle\ ,\ \rangle_D$ and $\langle\ ,\ \rangle_P$ denote the inner products in the data and parameter spaces, respectively. We assume that the inner products in the parameter space P and in the data space D are given by

$$\langle f, g \rangle_D = \sum_{j=1}^{N_p} \int_0^{t_f} f_j\, g_j\, dt\ ; \quad \langle A, B \rangle_P = \int_\Omega A\, B\, d\mathbf{x}\ , \tag{21}$$

where $f_j = f(\mathbf{x}_{p_j}, t)$ and $g_j = g(\mathbf{x}_{p_j}, t)$, $j = 1, \ldots, N_p$, are time functions defined at the production well positions $\mathbf{x}_{p_j}$. The following adjoint form of the linearized residual operator has been derived in [6].

Let $\rho \in D$ be an arbitrary function in the data space. Then $R'[K]^*\rho$ is given by

$$R'[K]^* \rho = \int_0^{t_f} \frac{T_w}{K} \nabla p \nabla z\ dt \tag{22}$$

where z is the solution of the adjoint equation

$$-\phi \frac{\partial z}{\partial t} + \frac{\partial T_w}{\partial S_w} \nabla p \nabla z - (z - \sum_{j=1}^{N_p} \rho\ \delta(\mathbf{x} - \mathbf{x}_j^{(p)})) \frac{\partial Q_w}{\partial S_w} = 0 \quad \textit{in } \Omega \tag{23}$$

$$z(\mathbf{x}, t_f) = 0 \quad \textit{in } \Omega, \tag{24}$$

and S_w and p are the solutions of (1)–(8).

Note that, as typical for the adjoint scheme, the system (23)–(24) physically models some kind of *backpropagation* with respect to the linearized forward model. The residuals are applied at the production wells as artificial injectors, and propagated backward in time (notice the minus sign in front of the time derivative in (23) and the prescribed final value conditions in (24), compared to a plus sign in (17) and initial values in (18)) and in space by the

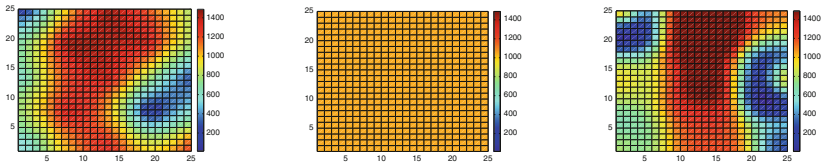

Fig. 2. Example of a reconstructed permeability distribution. *Left image*: reference profile. *Center image*: initial profile. *Right image*: reconstructed profile

system (23)–(24). Equation (22) uses these backpropagated fields to extract an update direction by combining forward and adjoint fields at each location.

In Fig. 2 we show an example of a reconstruction applying the adjoint method. The reference permeability distribution is shown in the left image. The well configuration used in this example is the same shown in Fig. 1. There is one injector well at the center of $600 \times 600\,\mathrm{m}^2$ reservoir and four producer wells at the corners. The reservoir is discretized by a 25×25 uniform spatial grid. Our initial model, shown in the center image, consists of a uniform permeability distribution of 1,040 mD. The estimated permeability distribution at the end of the 20th iteration is shown in the right image. We can observe a very good agreement between the reference and estimated permeability distributions.

3 Optical Molecular Imaging

Optical molecular imaging is showing great promise for monitoring several cellular and structural changes associated with predisease states such as dysplastic progression [7–10]. In this application, near-infrared fluorescent probes are used to mark specific cellular targets within the tissue that re-emit light upon excitation by an external light source. These markers act as internal sources that can be imaged from measurements of the light intensity at the tissue surface. The goal of determining the internal fluorescent source distribution from boundary measurements can be stated as an inverse source problem.

Several challenges arise in optical molecular imaging due to the multiple scattering of light in tissues. Physically, multiple scattering causes severe image blurring and, therefore, one cannot make use of direct images. Rather, one must develop methods to reconstruct images from scattered light measurements.

To model diagnostic measurements we use the radiative transport equation. It describes accurately light propagation in tissues [11–13]. To study the inverse fluorescent source problem we use the integral formulation of

this equation in three dimensions. Using the point source and voxel source solutions, we estimate the location, size and total strength of a general source [14].

3.1 The Direct Problem: The Radiative Transfer Theory

Modeling fluorescence in tissues must account for the following stages: (1) propagation of excitation light from the tissue's surface into its interior, (2) absorption by fluorophores, (3) conversion to fluorescence, (4) emission of the fluorescent light from the fluorophores, and (5) propagation of that light back up to the tissue surface. We assume here continuous illumination and that the absorption and emission spectra of the fluorescent molecules do not overlap. Hence, the excitation and emission processes take place at different wavelengths denoted by λ_x and $\lambda_m > \lambda_x$, respectively. Accordingly, the forward model describing the transport of excitation and emission light can be written as:

$$\mathbf{\Omega} \cdot \nabla I_x + (\mu_a^x + \mu_a^{x\to m}) I_x - \mu_s^x L I_x = 0, \tag{25}$$

$$\mathbf{\Omega} \cdot \nabla I_m + \mu_a^m I_m - \mu_s^m L I_m = S_{x\to m}. \tag{26}$$

In these equations, I_x (I_m) is the specific intensity for the exciting (emission) light at wavelength λ_x (λ_m). They depend on direction $\mathbf{\Omega} \in \mathbb{S}^2$ ($\mathbb{S}^2$ denotes the unit sphere) and position $\mathbf{r} \in \mathbb{R}^3$. At the excited (emission) wavelength λ_x (λ_m), the absorption and scattering coefficients are denoted by μ_a^x and μ_s^x (μ_a^m and μ_s^m), respectively. The absorption by fluorophores in (25) is given by the fluorophore absorption coefficient, $\mu_a^{x\to m}$. The isotropic source term

$$S_{x\to m}(\mathbf{r}) = \eta U_x(\mathbf{r}) \mu_a^{x\to m}(\mathbf{r}) \tag{27}$$

is the product of the quantum efficiency η of the fluorophore, the average excited intensity

$$U_x(\mathbf{r}) = \frac{1}{4\pi} \int_{\mathbb{S}^2} I_x(\mathbf{\Omega}, \mathbf{r}) \, \mathrm{d}\, \mathbf{\Omega}, \tag{28}$$

and the fluorophore absorption coefficient $\mu_a^{x\to m}$. This average excited intensity excites the fluorophore molecules from their ground state to an excited state. The quantum efficiency η quantifies the conversion to fluorescence.

The scattering operations $LI_{x,m}$ in (25) and (26) are defined as

$$LI_{x,m}(\mathbf{\Omega}, \mathbf{r}) = -I_{x,m}(\mathbf{\Omega}, \mathbf{r}) + \int_{\mathbb{S}^2} f_{x,m}(\mathbf{\Omega} \cdot \mathbf{\Omega}') I_{x,m}(\mathbf{\Omega}', \mathbf{r}) \, \mathrm{d}\, \mathbf{\Omega}'. \tag{29}$$

The scattering phase functions $f_{x,m}$ in (29) give the fraction of light scattered in direction $\mathbf{\Omega}$ due to light incident in direction $\mathbf{\Omega}'$ at wavelengths $\lambda_{x,m}$, respectively.

3.2 The Inverse Problem: A Semi-Analytical Method

The objective in optical molecular imaging is to reconstruct the fluorescent source $S_{x\to m}(\mathbf{r})$ in the domain D using measured data taken from the boundary surface ∂D. Since the coupling between (25) and (26) is only through the source term in (26), and the goal of our inverse problem is precisely to reconstruct it, we can consider only the second equation (26).

Because the only source of light in this problem is the fluorescent source, we prescribe boundary conditions of the form:

$$I_m(\mathbf{\Omega}, \boldsymbol{\rho}) = 0, \quad \mathbf{\Omega} \cdot \mathbf{n}(\boldsymbol{\rho}) > 0, \quad \boldsymbol{\rho} \in \partial D, \tag{30}$$

with $\mathbf{n}(\boldsymbol{\rho})$ denoting the *inward* normal at $\boldsymbol{\rho} \in \partial D$. Moreover, we impose that I_m is bounded everywhere in the halfspace. Our measured data R is the specific intensity at the boundary for all directions pointing out of D:

$$R(\mathbf{\Omega}, \boldsymbol{\rho}) = I_m(\mathbf{\Omega}, \boldsymbol{\rho}), \quad \mathbf{\Omega} \cdot \mathbf{n}(\boldsymbol{\rho}) < 0, \quad \boldsymbol{\rho} \in \partial D. \tag{31}$$

For the inverse fluorescent source problem, we wish to reconstruct the fluorescent source $S(\mathbf{r})$ with the measured data given by (31) and the direct problem given by (26) subject to (30). Here, we focus on the case of planar fluorescent reflectance imaging. The domain is modeled as a halfspace $D = \{z > 0\}$ bounded by the plane $\partial D = \{z = 0\}$. The halfspace is composed of a uniform absorbing and scattering medium. The constant absorption and scattering coefficients, denoted by μ_a and μ_s, respectively, are assumed to be known. The scattering phase function f is also assumed to be known.

In the method introduced in [14] we use the Green's function for the radiative transport equation and the general representation formula to find key properties of a fluorescent source such as its location an size. The Green's function is computed analytically as an expansion of plane wave solutions. The plane wave solutions are computed numerically. Using the Green's function for the radiative transport equation, we represent the measured data R as the superposition of interior sources and surface sources. With this representation, we can subtract off contributions from surface sources explicitly from the measured angular data yielding a quantity that depends only on the interior source of interest. Finally, we derive closed-form analytical solutions to recover a point source and a voxel source. For more details we refer the reader to [14].

We point out that the analysis in [14] relies on full angular measurements at the tissue boundary. However, one does not always have access to this data in general, but only to that given by the limited angular aperture of the detector. An extension to this theory to treat limited angular data can be found in [15].

In Fig. 3 we show the performance of our approach. We show results in which we estimate the location and size of general a fluorescent source

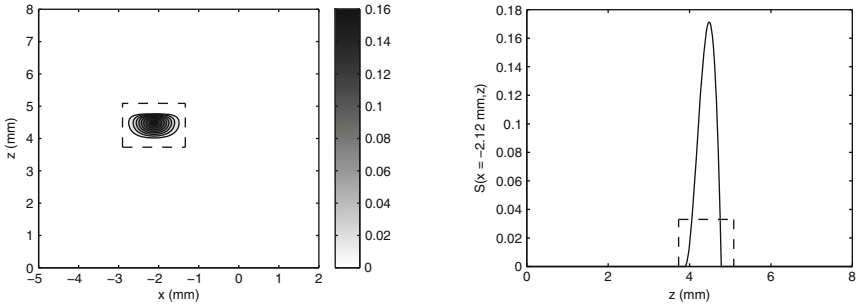

Fig. 3. Example of the estimation of the location and size of a general source. *Left plot*: contour of the true source and outline of the recovered pixel source. *Right plot*: slice of the source at $x = -2.1\,\text{mm}$ and the recovered pixel source. (From Kim and Moscoso [14])

$$S(x,z) = S_0\, e^{-(x-x_0)^2/w^2} \times \begin{cases} -(z-a)^2(z-b) & z \in [a,b], \\ 0 & \text{otherwise}, \end{cases} \tag{32}$$

by recovering the parameters of a pixel source. We consider a halfspace $z > 0$ composed of a uniform absorbing and scattering medium. The absorption and scattering coefficients are $\mu_a = 0.01\,\text{mm}^{-1}$, and $\mu_s = 1.0\,\text{mm}^{-1}$, respectively. We used the Henyey–Greenstein scattering phase function with asymmetry parameter $g = 0.8$. Hence, $\mu_s(1-g)/\mu_a = 20$ which is in the range of optical properties of tissues and tissue phantoms. The numerical simulations were computed in two dimensions: x and z.

The parameters used in (32) for the fluorescent source are: $S_0 = 1.64$, $x_0 = -2.1$, $w = 0.43$, $a = 3.89$ and $b = 4.78$. With these parameter values, the total strength, defined as

$$S_{total} = \int_0^\infty \int_{-\infty}^\infty S(x,z)\, dx\, dz, \tag{33}$$

is $S_{total} \approx 0.0654$.

The left plot in Fig. 3 shows the contours of the true source and the outline of the recovered pixel source. The middle plot shows the slice of the source at $x = -2.1\,\text{mm}$ and the recovered pixel source. The right plot shows the source at $z = 4.335\,\text{mm}$ and the recovered pixel source. The pixel that we recovered has parameter values: $S_0 = 0.033$, $x_1 = -2.9044$, $x_2 = -1.3356$, $z_1 = 3.7319$ and $z_2 = 5.0862$, so that the total strength recovered is $S_{total} = 0.0701$. We observe that the pixel source captures the correct location, the size, and the total strength of the source very well. Figure 3 validates our theory.

4 Conclusions and Further Work

In this paper we wanted to stress that imaging is more than showing that an inverse problem may have a unique solution under circumstances that are rarely satisfied in practice. Modern imaging approaches deal with understanding the trade off between data size, the quality of the image, the computational complexity of the forward model used to generate the measurements, and the complexity and stability of the numerical algorithm employed to obtain the images. One neither has all the data he wants, nor can solve a very general forward model to invert the data. Finally, progress can hardly be carried out without a deep understanding of the mathematical model with which we interpret the data and without efficient and well designed numerical algorithms to solve the mathematical model.

Acknowledgments

The author thanks his coauthors Oliver Dorn, Pedro González-Rodríguez, Manuel Kindelan and Arnold Kim for our extended collaboration on imaging and other interesting problems. The author also acknowledges support from the Spanish Ministry of Education and Science (grant no FIS2007-62673) and by the Autonomous Region of Madrid (grant no S-0505/ENE/0229, COMLIMAMS).

References

1. Suri, J.S., Farag, A.: Deformable Models: Theory and Biomaterial Applications, Springer, New York (2007)
2. Natterer, F., Wübbeling, F.: Mathematical Methods in Image Reconstruction. SIAM Monographs on Mathematical Modeling and Computation. SIAM, Philadelphia (2001)
3. Thomas, G. W.: Principles of Hydrocarbon Reservoir Simulation, Prentice-Hall, New Jersey (1982)
4. Villegas, R., Dorn, O., Moscoso, M., Kindelan, M., Mustieles, F.J.: Proceedings of the Paper C015, Society of Petroleum Engineers SPE-paper 1002911 (2006)
5. Villegas, R., Dorn, O., Moscoso, M., Kindelan, M.: Progress in Industrial Mathematics at ECMI 2006, vol. 12, pp. 597–602. (2006)
6. González-Rodríguez, P., Kindelan, M., Moscoso, M., Dorn, O.: Inverse Probl. **21**, 565–590 (2005)
7. O'Leary, M.A., Boas, D.A., Li, X.D., Chance, B., Yodh, A.G.: Opt. Lett. **15**, 158–160 (1996)
8. Hawrysz, D.J., Sevick-Muraca, E.M.: Neoplasia. **2**, 388–417 (2000)
9. Ntziachristos, V., Weissleder, R.: Opt. Lett. **26**, 893–895 (2001)
10. Graves, E.E., Ripoll, J., Weissleder, R., Ntziachristos, V.: Med. Phys. **30**, 901–911 (2003)
11. Moscoso, M., Keller, J.B., Papanicolaou, G.: J. Opt. Soc. Am. A. **18**(4), 948–960 (2001)

12. Kim, A.D., Keller, J.B.: J. Opt. Soc. Am. A. **20**, 92–98 (2003)
13. Kim, A.D., Moscoso, M.: J. Biomed. Opt. **10**, 034015 (2005)
14. Kim, A.D., Moscoso, M.: Inverse Probl. **22**, 23–42 (2006)
15. González-Rodríguez, P., Kim, A.D., Moscoso, M.: J. Opt. Soc. Am. A. **24**, 3456–3466 (2007)